

Identification of Prismatic Slip Bands in 4H SiC Boules Grown by Physical Vapor Transport

SEOYONG HA,¹ NOEL T. NUHFER,¹ GREGORY S. ROHRER,¹
MARC DE GRAEF,¹ and MAREK SKOWRONSKI^{1,2}

1.—Carnegie Mellon University, Department of Materials Science & Engineering,
5000 Forbes Avenue, Pittsburgh, Pennsylvania 15213, USA. 2.—e-mail: mareks@cmu.edu

Transmission electron microscopy (TEM) and KOH etching have been used to study the dislocation structure of 4H SiC wafers grown by physical vapor transport. A new type of threading dislocation arrays was observed. Rows of etch pits corresponding to dislocation arrays were observed in vicinity of micropipes, misoriented grains and polytypic inclusions at the periphery of the boules and extended along the $\langle 11\bar{2}0 \rangle$ directions. Plan view conventional and high resolution TEM showed that the arrays consisted of dislocations threading along the c-axis with Burgers vectors having edge components of the $a/3\langle 11\bar{2}0 \rangle$ type. The Burgers vectors were parallel to the corresponding arrays. The dislocation arrays were interpreted as slip bands formed by dislocation glide in the prismatic slip system $\langle 11\bar{2}0 \rangle \{ \bar{1}100 \}$ of hexagonal SiC during post-growth cooling.

Key words: Silicon carbide, bulk crystal growth, physical vapor transport, threading dislocation, prismatic slip

SiC is a wide band gap semiconductor material uniquely suited for high power, high temperature, and high frequency electronic devices. Many of its properties are superior to those of Si and GaAs.¹⁻⁵ In recent years, significant progress in SiC bulk crystal growth has enabled the fabrication of large diameter high quality substrates suitable for SiC based devices. However, most SiC substrates still contain relatively high densities of structural defects such as micropipes, dislocations, and inclusions, which will have to be reduced in order to improve the yields of device fabrication. Of particular interest are extended defects propagating along the [0001] growth direction. Such threading defects are known to penetrate active device layers deposited by epitaxy and to deteriorate device performance.⁶⁻¹⁰

In previous studies, three characteristic etch pit types were observed on the surfaces of [0001] grown SiC crystals and assigned to three different threading defects. The largest pits (20–30 μm) were hexagonal in shape and corresponded to micropipes.¹⁰⁻¹⁵ Medium (10–20 μm) and small (below 10 μm) pits were hexagonal or round in shape, depending on the wafer face polarity and/or the doping concentration.¹¹ The former type was ascribed to threading screw dislocations

with Burgers vectors of the $1c[0001]$ type.^{10,11} The latter was attributed to threading edge dislocations with Burgers vectors of the $a/3\langle 11\bar{2}0 \rangle$ type. The threading edge dislocations frequently formed arrays of etch pits extending along the $\langle 1100 \rangle$ directions on etched basal plane cut SiC wafers. The arrays were interpreted as domain walls, which are known to exist in silicon carbide boules grown by physical vapor transport.^{16,17} Contrast analysis of the domain wall in x-ray topography images indicated that Burgers vectors of the dislocations in the wall are perpendicular to the wall.¹² Such arrangement corresponds to a low energy configuration because a tensile stress field of an edge dislocation is positioned on top of the compressive stress field of the neighboring dislocation compensating each other. This leads to elimination of long range stress fields. Analysis of SiC boules sliced along the [0001] growth direction showed that the domain structure was grown-in and originated in the seed crystal. High resolution x-ray diffraction measurements indicated that the domain boundaries have both a twist and a tilt component of misorientation.¹² In this letter, we report the observation of a new type of threading dislocation array extending along the $\langle 11\bar{2}0 \rangle$ directions. Both the morphology and origin of the arrays are different from those of the domain walls reported earlier.¹⁰⁻¹²

(Received November 16, 1999; accepted March 31, 2000)

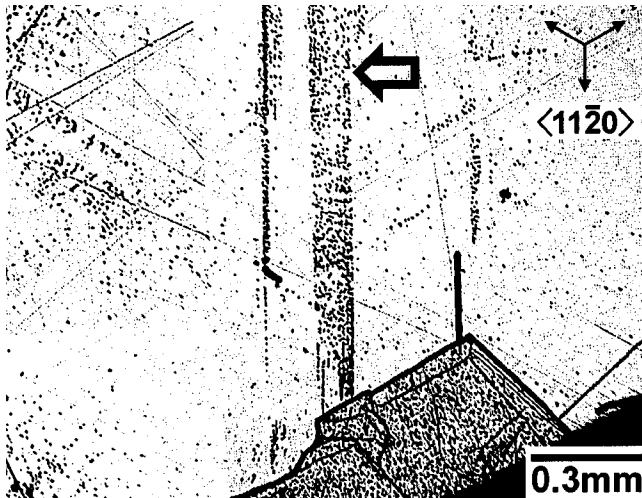


Fig. 1. Optical micrograph of the etch pit bands on KOH etched Si(0001) face of a 4H SiC wafer. The arrow points to the most pronounced band.

The crystals used in this study were grown by Cree Research, Inc. (Durham, NC) as a part of the development program on high temperature electronics, supported by the Defense Advanced Research Project Agency. The wafers were undoped or n-doped and [0001]-oriented to within 0.5° . Chemical wet etching in molten KOH was used to reveal the defect structure. All wafers were etched at 500°C or 510°C for 10 min. The etch pits were observed using Nomarski-contrast optical microscopy and classified with respect to their morphology. The specimens for Transmission Electron Microscopy (TEM) observations were cut from specific areas of the wafers and lapped down to a thickness of about $100\ \mu\text{m}$ with boron carbide abrasive powder. They were then dimpled to a thickness of about $20\ \mu\text{m}$ with $6\ \mu\text{m}$ diamond paste. Finally, the samples were sputtered by Ar^+ beam in a Gatan Precision Ion Polishing System to obtain electron transparency. The TEM observations were carried out on a Philips EM420-TEM and on a JEOL 4000 EX-TEM, operated at 120 kV and 400 kV, respectively.

Figure 1 is an optical micrograph of an etched Si(0001) face of a 4H SiC wafer. The wafer edge is visible in the lower right corner of the figure and a part of a polytypic inclusion or a misoriented grain at the edge of the wafer is shown in the lower center. The most apparent features in this figure are the two parallel bands of small etch pits extending from the bottom to the top of the figure. Their full lengths were about 4 mm and 10 mm, respectively (the wider of the two bands is marked with an arrow in Fig. 1). It is also noticeable that there are several additional less well defined bands of pits rotated 60° away from the dominant bands. The widths of the bands were between $30\ \mu\text{m}$ and $200\ \mu\text{m}$. The etch pit densities in the bands were in the range of $0.5\text{--}2.2 \times 10^6\ \text{cm}^{-2}$. Laue x-ray diffraction was used to determine the orientation of the bands. All of them extended along the $\langle 11\bar{2}0 \rangle$ directions. This is also evident in Fig. 2, which is a magnified image of the smaller of the two large bands.

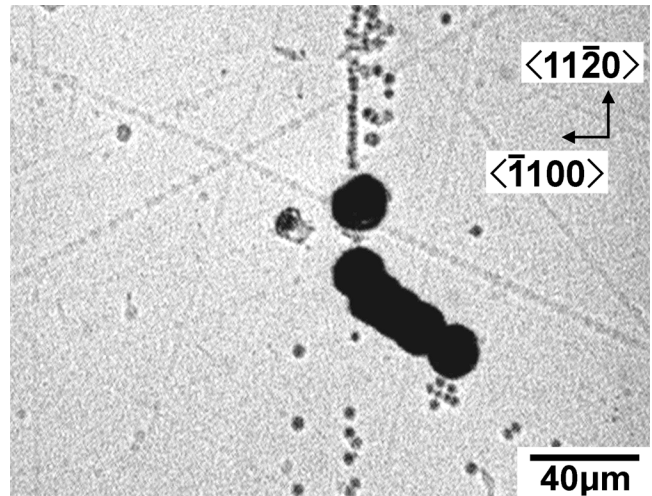


Fig. 2. Magnified optical micrograph showing hexagonal etch pits of micropipes and an etch pit band. The band is running parallel to one of the three equivalent sides of the hexagon.

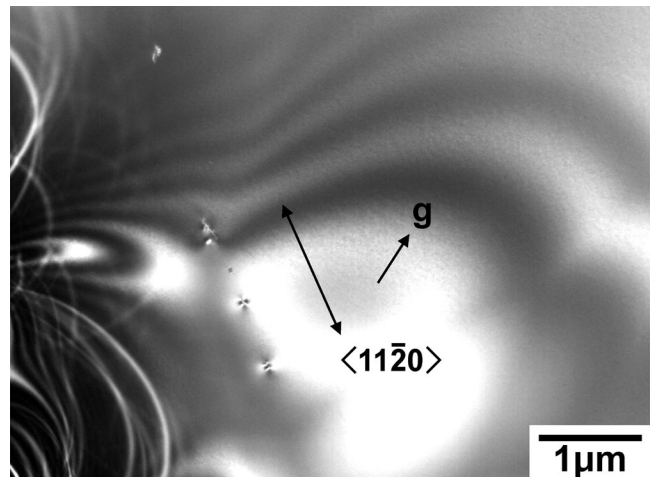


Fig. 3. Plan view bright field conventional TEM micrograph showing a part of a dislocation array shown in Fig. 1 ($\mathbf{g} = [2110]$).

The large hexagonal etch pits located in the center of Fig. 2 were formed at the emergence points of micropipes.^{10–15} It is clear that the band direction is parallel to one of the three equivalent sides of the hexagonal pits, of which the directions are of the $\langle 11\bar{2}0 \rangle$ type.¹² In the figure, most small etch pits show regular circular shapes on the surface, which implies that these are due to threading dislocations approximately normal to the basal plane and wafer surface. In particular, they are different from the shell etch pits assigned to basal plane dislocations by Takahashi et al.¹¹ The etch pit bands shown in Fig. 1 are clearly different from the previously reported domain walls since they extend along different crystallographic directions. We have used conventional and high resolution TEM to determine the character (line direction and Burgers vector) of the dislocations in the bands.

Figure 3 is a plan view conventional TEM image showing a part of a band shown in Fig. 1. Five dislocations are visible in the figure forming a straight

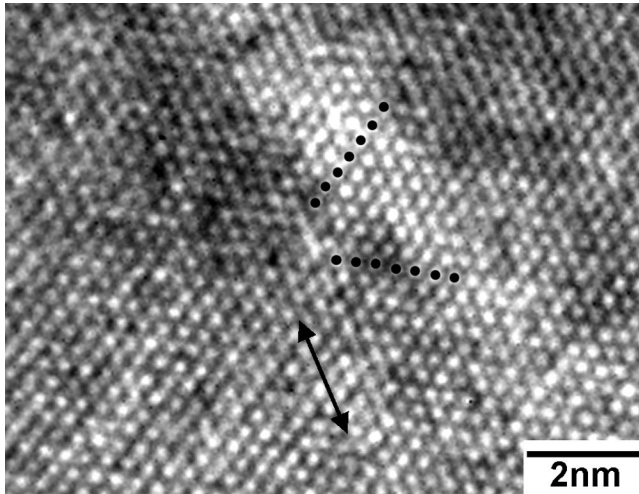


Fig. 4. C-axis plan view lattice image around a dislocation in the array of Fig. 3. The two extra half planes are marked with two arrays of dots and the corresponding edge component direction of the Burgers vector with an arrow.

array along a $[11\bar{2}0]$ direction. This image was taken in a two beam diffraction condition with $\mathbf{g} = [\bar{2}110]$. The fact that the lattice distortion contrast features due to the dislocations are nearly point-shaped implies that the dislocation lines are almost parallel to the c-axis. In a plan view sample with dislocation line perpendicular to the sample surface, it is very difficult to apply regular $\mathbf{g} \cdot \mathbf{b}$ contrast analysis to determine the Burgers vector direction. Such information can be obtained from cross sectional samples. However, the low dislocation density in the arrays makes the cross sectional sample preparation exceedingly difficult. Thus, high resolution TEM was applied to determine the line directions and Burgers vectors of the individual dislocations more precisely though it can only determine the components of Burgers vectors perpendicular to the beam direction. Figure 4 is a plan view high resolution lattice image around a dislocation in the array shown in Fig. 3. The image was taken by choosing the c-axis as the zone axis. The dislocation is threading along the c-axis without tilt. Its core is at the intersection of the two extra half planes marked with two rows of dots. The corresponding edge component of the Burgers vector, determined by drawing a Burgers circuit around the core, is $a/3[11\bar{2}0]$ with a direction marked with an arrow. The dislocation array and the edge components of the individual dislocations in it were determined to be parallel to each other by means of careful alignment of conventional low magnification diffraction contrast images and high resolution TEM images.

The type of dislocations making up the array, the relationship between their Burgers vector and the array direction, and the array morphology are consistent with a slip band generated by the prismatic slip: $\langle 11\bar{2}0 \rangle \{1100\}$. At initial stages of single crystal deformation, relatively few dislocation sources are operative. New dislocations will be multiplied at the sources and glide in the plane determined by their Burgers vector and line direction. Repeated multiplication

would generate an array parallel to the Burgers vector as observed in the above experiments. It should be pointed out, that such arrangement of dislocations corresponds to a high energy configuration because the strain fields of individual dislocations add up and create long range stress fields. It is highly unlikely that such array could be grown-in. Also, the grown-in dislocations are typically between misoriented subgrains nucleated and grown independently, and form low angle grain boundaries.^{18,19} The $\langle 11\bar{2}0 \rangle$ arrays discussed here are not misorientation boundaries like the low angle boundaries. Another characteristic feature of the $\langle 11\bar{2}0 \rangle$ arrays is their width (30~200 μm in Fig. 1). Glide dislocations typically do not lie in one glide plane but in a set of parallel planes with widening caused by multiple cross glide.²⁰ All of the above characteristics lead us to interpret the origin of the arrays as the prismatic slip. It is well known that the primary mechanism of SiC deformation is the basal plane slip: $\langle 11\bar{2}0 \rangle (0001)$.²¹⁻²³ While the activation of the secondary slip is more difficult, it has been observed experimentally by Maeda et al.²² TEM images of samples indented at room temperature show dislocation loops with $\langle 11\bar{2}0 \rangle$ and $[0001]$ segments. This indicates that while the Peierls energy in SiC is significant, the activation of secondary slip systems is possible. Considering the fact that the Peierls stress decreases with increasing temperature, it should be much easier to activate the secondary slip while cooling from the growth temperature (~2300°C) than at room temperature. Similar dislocation etch pit arrays (the arrays were along the $\langle 11\bar{2}0 \rangle$ directions on etched basal plane surfaces) were reported by Amelincx et al.²⁴ in SiC crystals grown by the Lely method. They interpreted them as glide traces in a pyramidal slip system $\langle 11\bar{2}0 \rangle \{3\bar{3}01\}$ forming dislocation pile-ups against a screw dislocation or screw dislocation groups. We presented here more direct and systematic evidence of secondary slip in SiC.

As illustrated in Fig. 1, the apparent origins of most slip bands are misoriented grains or polytypic inclusions at the periphery of the wafers. The grains or inclusions are frequently observed to nucleate on the growth crucible walls. During post-growth cooling, the thermal expansion anisotropy between the matrix boule and the misoriented grains leads to stress build-up at the interface as well as inside the grains and the boule. Similarly, any polytypic inclusions would result in stresses due to differences in thermal expansion. As the temperature decreases, the stresses will increase until they exceed the critical resolved shear stress and activate the dislocation glide in the corresponding slip system.

In summary, threading dislocations forming etch pit bands along the $\langle 11\bar{2}0 \rangle$ directions on Si(0001) faces of $[0001]$ grown crystals were shown to lie along the c-axis with Burgers vectors having edge components of the $a/3\langle 11\bar{2}0 \rangle$ type. The bands are formed by glide of these dislocations in the prismatic slip system $\langle 11\bar{2}0 \rangle \{1100\}$ during post-growth cooling.

This work was supported in part by the Common-

wealth of Pennsylvania through the Ben Franklin Technology Center (Grant No. 98W.CM00562R-1) and by National Science Foundation (Grant No. DMR.9903702).

REFERENCES

1. M. Bhatnagar and B.J. Baliga, *IEEE Trans. Electron Dev.* 40, 645 (1993).
2. T.P. Chow and M. Ghezzi, *Mater. Res. Soc. Symp. Proc.* 423, 9 (1996).
3. C.E. Weitzel and K.E. Moore, *Mater. Res. Soc. Symp. Proc.* 483, 111 (1998).
4. B.J. Baliga, *Mater. Res. Soc. Symp. Proc.* 512, 77 (1998).
5. C.E. Weitzel, *Mater. Sci. Forum* 264-268, 907 (1998).
6. P.G. Neudeck and J.A. Powell, *IEEE Electron Dev. Lett.* 15, 63 (1994).
7. G. Gradinaru, M. Helmi, Y. Khlebnikov, G. Korony, W.C. Mitchel, and T.S. Sudarchan, *Mater. Res. Soc. Symp. Proc.* 442, 643 (1997).
8. U. Zimmermann, A. Hallén, A.O. Konstantinov, and B. Breitholtz, *Mater. Res. Soc. Symp. Proc.* 512, 151 (1998).
9. P.G. Neudeck, W. Huang, and M. Dudley, *IEEE Trans. Electron Dev.* 46, 478 (1999).
10. K. Koga, Y. Fujikawa, Y. Ueda, and T. Yamaguchi, *Amorphous and Crystalline Silicon Carbide IV, Springer Proc. in Physics* 71, 96 (1992).
11. J. Takahashi, M. Kanaya, and Y. Fujiwara, *J. Cryst. Growth* 135, 61 (1994).
12. J. Takahashi, N. Ohtani, and M. Kanaya, *J. Cryst. Growth* 167, 596 (1996).
13. J. Takahashi and N. Ohtani, *phys. stat. sol. (b)* 202, 163 (1997).
14. N. Sugiyama, A. Okamoto, K. Okumura, T. Tani, and N. Kamiya, *J. Cryst. Growth* 191, 84 (1998).
15. N. Ohtani, J. Takahashi, M. Katsuno, H. Yashiro, and M. Kanaya, *Mater. Res. Soc. Symp. Proc.* 510, 37 (1998).
16. R.C. Glass, L.O. Kjellberg, V.F. Tsvetkov, J.E. Sundgren, and E. Janzén, *J. Cryst. Growth* 132, 504 (1993).
17. M. Tuominen, R. Yakimova, R.C. Glass, T. Tuomi, and E. Janzén, *J. Cryst. Growth* 144, 267 (1994).
18. W. Qian, M. Skowronski, M. De Graef, K. Doverspike, L.B. Rowland, and D.K. Gaskill, *Appl. Phys. Lett.* 66, 1252 (1995).
19. B. Heying, X.H. Wu, S. Keller, Y. Li, D. Kapolnek, B.P. Keller, S.P. DenBaars, and J.S. Speck, *Appl. Phys. Lett.* 68, 643 (1996).
20. D. Hull and D.J. Bacon, *Intro. to Dislocations*, 3rd ed. (Oxford, U.K.: Butterworth-Heinemann, 1984), p. 179.
21. S. Fujita, K. Maeda, and S. Hyodo, *Phil. Mag. A* 55, 203 (1987).
22. K. Maeda, K. Suzuki, S. Fujita, M. Ichihara, and S. Hyodo, *Phil. Mag. A* 57, 573 (1988).
23. A.V. Samant, W.L. Zhou, and P. Pirouz, *phys. stat. sol. (a)* 166, 155 (1998).
24. S. Amelinckx, G. Strumane, and W.W. Webb, *J. Appl. Phys.* 31, 1359 (1960).